Energy dissipative mechanism of graphene foam materials

Chao Wang [a], Douxing Pan [b], Shaohua Chen [c, d, e, *]

[a] LNM, Institute of Mechanics, Chinese Academy of Sciences, Beijing, 100190, China
[b] Institute of Advanced Manufacturing Technology, Hefei Institutes of Physical Science, Chinese Academy of Sciences, Changzhou, 213164, China
[c] Institute of Advanced Structure Technology, Beijing Institute of Technology, Beijing, 100081, China
[d] Beijing Key Laboratory of Lightweight Multi-functional Composite Materials and Structures, Beijing Institute of Technology, Beijing, 100081, China
[e] Collaborative Innovation Center of Electric Vehicles in Beijing, Beijing Institute of Technology, 100081, China

ARTICLE INFO

ABSTRACT

Graphene foam (GrF) is a new kind of multi-porous material with many potential applications owing to its excellent multi-functional properties, especially its dissipation capability. However, both the dissipative mechanism and some experimental phenomena remain poorly understood. Here, systematic coarse-grained molecular dynamic simulations (CGMD) are conducted to study these issues. The typical stress-strain relationships found in experiments under large-strain loading-unloading and small-strain cyclic load are first reproduced. Based on microstructure analysis, three major dissipative mechanisms in the scale of flakes, i.e., rippling, sliding and impacting, are uncovered. The influencing effects of cycle number, strain magnitude and loading rate on dissipation are further investigated. It is found that the much higher dissipation in the first loading cycle is essentially due to drastic flake rearrangements, which decreases to a smaller one in subsequent cycles. In addition, the dissipation increases almost linearly with the strain magnitude in the first cycle, while it increases with a reduced slope in subsequent cycles due to the flake stacking structures. For a given strain magnitude, the dissipation will be enhanced as the loading rate increases. These results deepen our understanding on the dissipative mechanism of GrFs and should be helpful for the development of novel multi-functional graphene-based composites.

© 2018 Elsevier Ltd. All rights reserved.

1. Introduction

Graphene foam (GrF) [1–3], as a new kind of nano-porous material with three-dimensionally (3D) interconnected constituent graphene flakes, has attracted much attention in recent years, which has been proved possessing excellent properties of super-low density [4], super-elasticity [1,2,4], good electrical conductivity [5], electrochemical stability [6] and high energy dissipation [2]. These combined properties enable GrF many potential applications in damping materials [2], sensing [5], lithium ion batteries [6], sorbent materials [7], stretchable electronics [8], etc.

Most efforts have been dedicated to fabricating graphene foams with advanced properties by elaborate design of microstructures. Different synthetic methods and techniques would form GrFs with different properties. Both mechanical and electrical properties of as-synthesized graphene foams have been characterized and evaluated [1–3,8,9]. In mechanical aspects, some foams exhibit a rubber-like constitutive response under compression with three distinct regions, i.e., an elastic region, a collapse plateau and a densification region. A scaling law [10] has been derived for 3D GrFs, revealing that the compressive strength, the tensile strength and the Young's modulus are functions of density with the approximate power exponents 3.01, 2.01 and 2.73, respectively. A deformation characteristic of a near-zero [2] or a tunable Poisson's ratio [1] in a wide range $-0.30 < \nu < 0.46$ has been observed, showing a complex micro-structure-macro-property relationship induced by the micro-structure evolution. The impressive super-elasticity [1–4,11] that the foam materials could recover up to 90% compressive deformation and sustain their structural integrity under many loading cycles has been obtained experimentally. Some GrFs possess viscoelastic properties, whose storage/loss modulus and the damping ratio (ratio of the loss modulus to the storage modulus) [2,12] are found insensitive to the ambient temperature and the loading frequency, much different from the conventional elastomers like silicone rubber. The hysteresis loops of stress-strain curves in many cyclic loading-unloading experiments [1,3,4,13,14] have clearly revealed the strong dissipative

---

* Corresponding author. Institute of Advanced Structure Technology, Beijing Institute of Technology, Beijing, 100081, China.
E-mail addresses: chenshaohua72@hotmail.com, shchen@bit.edu.cn (S. Chen).

capability of GrFs, as well as the finite value of the damping ratio under small-strain cyclic load [2,12,15]. In the aspect of electrical property, their electrical resistance [3,8,13,14] has been found almost linearly depending on the loading strain and changes when repeatedly compressed up to 50% of strain for over 10 cycles. However, the electrical property of graphene foams is out of the scope of the present paper.

In contrast to a large number of experimental studies on the mechanical property of graphene foams, few theoretical and computational studies were carried out to evaluate the relationship between the macro-mechanical features and the intrinsic micro/nanostructures. Using full-atom molecular dynamic simulations, Baimova et al. [16] found that the nanostructures and mechanical properties of bulk amorphous graphene assembly could be altered by shear deformation at a high temperature, leading to the formation of structural rearrangements that cannot be destroyed by further deformation and annealing. Wang et al. [17] correlated the rubber-like constitutive relationship of GrFs under compression with the microstructural evolutions by CGMD and found that the flake thickness and compressive strain are two key factors controlling the Poisson's effect. Combining a bottom-up computational modeling with experiments based on 3D-printed models, Qin et al. [10] found that 3D graphene assembly has an exceptionally high tensile strength, which is 10 times as strong as a mild steel, but with a relatively low density of 4.6% that of the mild steel. Using in-situ SEM, Nieto et al. [18] conducted nano-indentation and uniaxial tension experiments to study the deformation mechanisms of graphene foams, in which they unveiled two main multi-scale deformation behaviors of flake bending and cell-wall elastic depression and obtained the multi-peak tensile stress-strain relationship and the ductile fracture mode. Pan et al. [19] showed that the macroscopic multi-peak stress-strain relationship is induced by the microscopic intermittent bond-breaking of flakes and physical crosslinks, and also successfully explained the fracture mode of near 45°plane from the tensile direction by analyzing the distribution and evolution of local stress state using the mesoscopic simulations and the macroscopic continuum fracture theory.

For the energy dissipative behavior of GrFs, although their dissipative capability has been repeatedly confirmed by the large-strain loading-unloading test [1,3,4,13,14] and the small-strain compression-tension cyclic load test [2,12], the microscopic dissipative mechanism is still unclear. To our best knowledge, only two works done by Debrupa et al. [20] and Pranjal et al. [15] are most related to this topic. However, Debrupa et al. [20] investigated the dissipative behavior of a few-layered graphene membrane rather than bulk graphene foams, and attributed the governing mechanism of energy dissipation to structural ripple formation and ripple wave propagation. Since bulk graphene foams are assembled by lots of building blocks of one- or a few-layered graphene membrane, the energy dissipative mechanism of which should be more beyond that of the membranes due to additional interactions among constituent flakes. Pranjal et al. [15] speculated that there probably exists an additional new mechanism of "flexing of foam branches" in the larger anatomical scale of branches/walls. However, it is just a speculation on the basis of the macroscopically experimental results, and no further explanation was given on how the energy is dissipated in such a larger scale of branches by solid experimental or numerical evidence. Moreover, considering the fact that branches/walls are composed of massive graphene flakes, the dissipation in the scale of branches/walls should be an integrated result of the basic dissipation in the smaller scale of flakes. Therefore, a comprehensive investigation in the scale of flakes is undoubtedly needed to understand the dissipative micromechanisms of graphene foams.

In addition, several experiments under large-strain compression-tension cyclic loads have shown that the dissipative energy is much larger in the first loading cycle than that in the subsequent cycles. Furthermore, the dissipative energy would keep almost constant after the first loading cycle [1,3,4,13]. Both questions of what the microstructural evolution is and how the microstructural evolution influences the energy dissipation under cyclic load are needed to answer too.

In this paper, the two-dimensional (2D) mesoscopic graphene model [21] was expanded into a 3D model of GrFs to study the microstructural mechanisms of energy dissipation and the corresponding evolving features under cyclic load. The 3D model has been successfully implemented to study the mechanical behaviors of graphene foams under uniaxial compression and tension loads in our previous works [17,19], where a series of mechanical phenomena were well explained, such as the rubber-like compressive constitutive responses, the near-zero Poisson's ratio, the multipeak tensile stress-strain curves and the fracture mode near 45°plane from the tensile direction as mentioned above. The rest of this paper is organized as follows. Section 2 introduces the numerical model of graphene foams as well as the methodology in this paper. The dissipative phenomena of GrFs are first reproduced under both larger-strain loading-unloading cycles and small-strain compression-tension cyclic load in Section 3. Then, the unified energy dissipative micro-mechanisms of GrFs under different loading forms are unveiled and a series of experimental phenomena on the energy dissipation are explained. Conclusions will be given finally at the end of this paper.

2. 3D numerical sample of GrF

Based on the equivalent energy principle and systematically full atomic calculations, a 2D coarse-grained mesoscopic model for a graphene sheet was established by Cranford and Buehler [21]. In the 2D mesoscopic model, each coarse grain (bead) represents a 2.5×2.5 nm^2 atomically single- or multilayer graphene sheet. A harmonic spring potential $\phi_T = k_T(r-r_0)^2/2$ is used to describe the axial stretching energy among all pairs of bonded particles, where k_T denotes a spring constant and r is the distance between two particles with an equilibrium distance $r_0 = 2.5$ nm. A harmonic rotational-spring potential $\phi_\varphi = k_\varphi(\varphi-\varphi_0)^2/2$ is used to describe the in-plane bending energy, where k_φ denotes the spring constant related to the bending angle φ among three particles with a referenced equilibrium angle $\varphi_0 = 90°$. $\phi_\theta = k_\theta(\theta-\theta_0)^2/2$ denotes the out-of-plane bending energy with a spring constant k_θ, where θ denotes the bending angle among three particles with a referenced equilibrium value $\theta_0 = 180°$. Using these three potential energy functions, the tensile deformation, the in-plane shear and out-of-plane bending deformation of graphene sheet could be well described by this coarse-grain model.

The π-π interaction is a kind of non-bonding interaction, responsible for the adhesion of neighbor graphene sheets and the further self-assembly to be graphene foams. It is described by a Lennard-Jones potential $\phi_{LJ} = 4\varepsilon((\sigma/r)^{12}-(\sigma/r)^6)$, where ε is a parameter determining the depth of the potential well, σ is a length scale parameter that determines the position of the minimum potential, and r is the bead-to-bead distance between different flakes. The corresponding coarse-grained parameters are given in Table 1. The similar description of π-π interaction has also been used in other coarse-grain schemes [22−24] of graphene sheet.

A 3D coarse-grained graphene foam model is established based on the 2D coarse-grained mesoscopic model. As a building block, the side length of each square coarse-grained flake is 25 nm, which contains one hundred beads as shown in Fig. 1a. All flakes are placed randomly in a big cubic box to ensure no interaction among them first. Then, NPT assemble technique is adopted to deal with

Table 1
The force field parameters for the coarse-grained model from Ref. [21].

Parameters	k_T	r_0	k_φ	φ_0	k_θ	θ_0	σ	ε
Value	3720	25	134960	90°	933087	180°	23.84	473
Units	kcalmol^{-1}Å^{-2}	Å	kcalmol^{-1}rad^{-2}	—	kcalmol^{-1}rad^{-2}	—	Å	kcalmol^{-1}
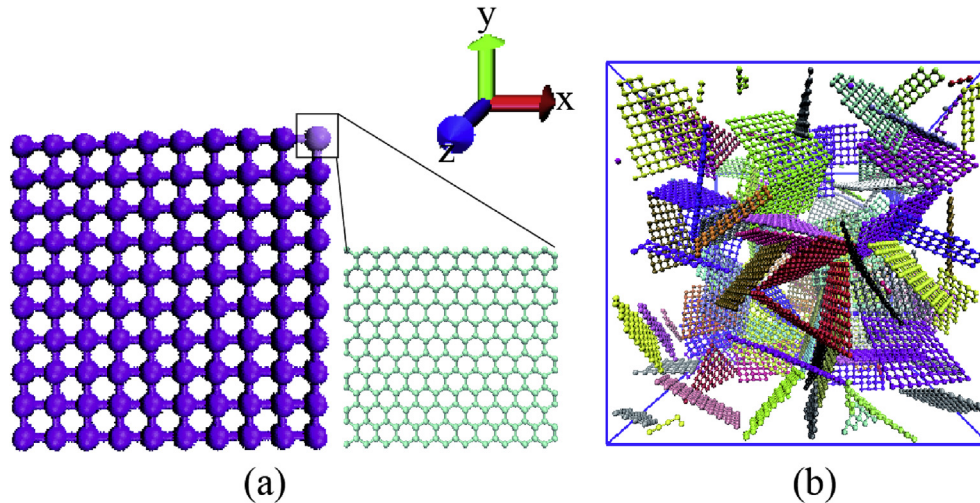
Fig. 1. Schematic of the simulation model. (a) A flake composed of coarse-grained graphene sheets. (b) The relaxed configuration of a coarse-grained graphene foam material. (A colour version of this figure can be viewed online.)

the system with a periodic boundary condition in three directions as well as a constant temperature 300 K and one barometric pressure. As a result, the system shrinks gradually and finally reaches an equilibrium state at about 30 ns with a time step 1 fs. Then, the ambient pressure is reset to zero. Under the berendsen barostat 0 Pa and Langevin thermostat 300 K, the system expands slightly and reaches the final equilibrium state at about 500 ns with the criterion that the total energy fluctuation converges to less than 1%. The final configuration is shown in Fig. 1b, in which the flakes are randomly oriented. In real experimental samples, the number of graphene layer in each flake is undetermined, but most of them contain 1-10 graphene layers [8,18,25]. Specially, the GrF used in Chae et al. [26] indicates about 8–10 graphene layers in one flake. For simplicity, in the present numerical model, all flakes are assumed to be identical, and a series of simulations for systems assembled by graphene flakes consisting of 1–10 graphene layers have been conducted. The stiffness of graphene flakes would become large along with the increasing number of graphene layers. The simulation results of the system with 8 graphene layers are mainly presented in this work. The size of flakes in experiments varies from several nanometers [10] to micrometers [2], which yields the corresponding equilibrium density of GrFs in a range of 1–100 mg/cm^3 [2,8,25]. It has been found that the equilibrium density of GrFs would decrease with an increasing flake size [17]. Considering the computational cost, we adopt a relatively small flake with the side length 25 nm in most of our numerical calculations and the corresponding equilibrium density of the numerical system is about 475 mg/cm^3. In addition, we do not consider the effect of strong chemical crosslinks among flakes in most of the simulations if not specified, which will mainly influence the elastic behavior of the numerical system. It should be noted that the apparent phenomenon that graphene flakes seem to be "rigid without bend" in Fig. 1b is due to the adopted graphene flakes with a relatively large stiffness. The case with relatively flexible graphene flakes can be found in Fig. S1, where the bending deformation is very obvious.

The structure of randomly distributed graphene sheets is chosen here as the numerical model for two reasons: 1) besides the regular honeycomb-like structure, the structure of randomly distributed graphene sheets is another general one, which can be fabricated by the other methods, such as the modified conventional hydrothermal method [2] or the template method [18]; 2) in the cell-wall level, whether in the honeycomb-like porous graphene foams [3] or in the other kind of porous graphene foams [11,27], the cell-wall itself consists of randomly distributed graphene flakes to some extent.

All the simulations are implemented with an open source software Large-scale Atomic/Molecular Massively Parallel Simulator (LAMMPS) [28].

3. Macroscopic behavior of GrFs under different loading forms

In order to disclose the dissipative micro-mechanism, the macroscopic behaviors of GrFs that have been widely observed in experiments with different loading conditions [1–4,12–14] are reproduced first, including the small-strain compression-tension cyclic load, the large-strain compression-unloading and the large-strain compression-tension-unloading.

First, the case of small-strain compression-tension cyclic loading is considered, which has been studied experimentally [2,15]. A sinusoidal strain load $\varepsilon = \varepsilon_0 \sin(\omega t)$ is adopted to act in the x-direction of the sample shown in Fig. 1b. As a result, a corresponding sinusoidal response of stress $\sigma = \sigma_0 \sin(\omega t + \delta)$ with a lag phase angle δ is activated as shown in Fig. 2, where ε_0 and σ_0 are the amplitude of strain and stress, respectively. ω and t are the loading frequency and the loading time, respectively. The damping ratio calculated by $\tan\delta$ is used as a measurement of the capability of energy dissipation. The damping ratio is obtained to be about 0.7 as the strain magnitude ε_0 and the loading frequency ω are set to be 0.011 and
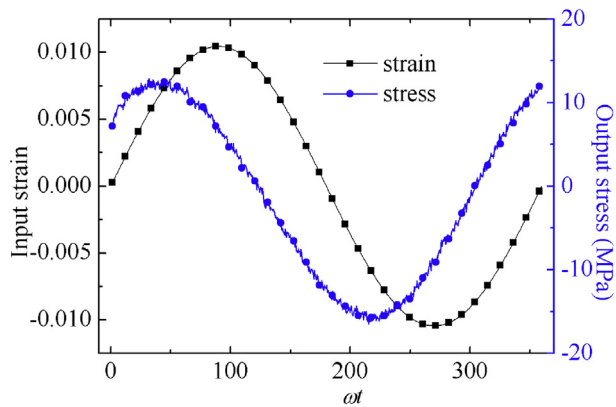
Fig. 2. The input cyclic compression-tension strain and the output stress as a function of the phase degree under a loading frequency of 1 GHz and temperature 300 K. (A colour version of this figure can be viewed online.)

10^9 s^{-1}, respectively. Compared with that in the graphene membranes [20], graphene foams [2] or CNT network materials [29], such a large damping value indicates a strong dissipation capability of the present simulation sample under a small-magnitude oscillating load as well. It shows that the present graphene foam material should have a viscoelastic property under a small-strain load. In order to verify this issue, we further consider a small-strain compression-unloading case, in which a compression strain is acted on the sample till the maximum value of 0.011, then the strain is unloaded and the sample is relaxed with enough time. The loading-unloading curve corresponding to the small-strain compression-unloading case is shown in Fig. 3. It is found that the graphene foam material exhibits obviously viscoelastic plastic property. The visco-deformation would be much larger than both the elastic and the plastic deformation if the loading strain is relatively small.

We further investigate the macroscopic behavior of the present numerical sample with the load form of large-strain compression-unloading. The well-equilibrated numerical sample is compressed uniaxially in the x-direction to a strain magnitude 0.31, then we remove the external compression and let the sample recover freely for a long time of 3 ns to a final stable state that the size of the sample is no longer changed. The result is given in Fig. 4a, where some corresponding snapshots are also shown for understanding.
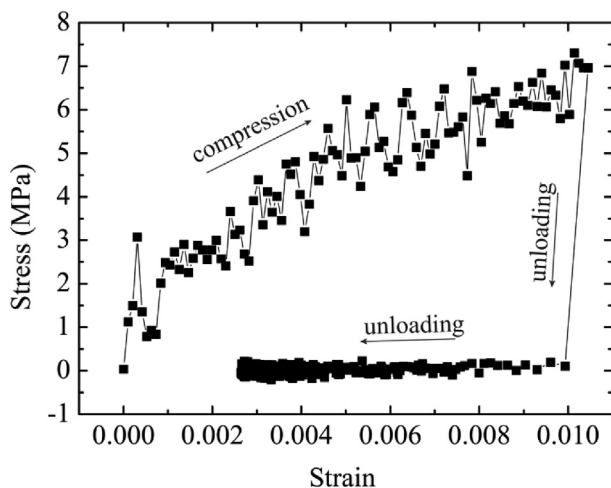
Fig. 3. The stress-strain constitutive relation of graphene foam materials under a small-strain compression-unloading condition.

Comparing the final configuration (snapshot 4) to that of the initial one (snapshot 1) shows a failed recovery. Only minor strain recovers due to the viscoelastic property and up to 90% total compressive deformation is left due to the large plastic deformation. The corresponding movie named "compression-unloading.gif" is provided in Supplementary Materials. It means the present sample will undergo much larger plastic deformation than both the visco and the elastic deformation under a large-strain compressive load.

Supplementary video related to this article can be found at https://doi.org/10.1016/j.carbon.2018.02.085.

As for the case with a loading form of large-strain compression-tension-unloading, a compressive strain is uniaxially added on the initially well-equilibrated system till 0.31, then the sample is tensioned in the reverse direction to its initial size at the same strain rate. During the tension process, the compressive stress decreases much quickly from a positive value to a negative one and then keeps nearly unchanged to the end. Finally, the sample is relaxed for 3 ns to a zero stress state as shown in Fig. 4b. A hysteresis loop of the stress-strain curve is obtained accordingly. The energy dissipated per unit volume can be measured by the area enveloped in the loop, which is composed of two parts divided by a dashed line in Fig. 4b. The areas above and below the dashed line represent the energy dissipated by compression and tension, respectively.

4. Micro-mechanism of energy dissipation under loading and unloading

Massive irreversible microstructural evolutions in the scale of flakes are found in the large-strain loading-unloading process by comparing the locally microstructural configurations in the initial state, the maximum compressed one and the unloading one. As shown in Fig. 5, four typically irreversible microstructural evolutions are mainly found, including the departure of two contacting flakes (Fig. 5a), transformation from edge-surface contacting configuration to the surface-surface one (Fig. 5b), the variation of contacting areas between two surface-surface contacting flakes (Fig. 5c) and the change of contacting partners (Fig. 5d).

In the small-strain loading-unloading process as shown in Fig. 3, flake rearrangement and the above mentioned microstructural evolutions also happen. However, due to the weak plastic deformation and the dominant visco-recovery, the microstructural evolutions during loading process will be largely restored after unloading and relaxation of enough time. The length of the sample in the loading direction would recover to 95.4 nm due to the visco-recovery, in contrast to the initial size 95.7 nm. The movie of "small-strain compression-unloading.gif" is given in Supplementary Materials.

All the four kinds of microstructural evolutions responsible for plastic or visco deformation would dissipate plenty of energy. A series of numerical simulations are carried out, including graphene foam materials formed by flakes with thickness varying from 1 to 10 layered graphene sheets, side length varying from 25 to 125 nm. Furthermore, cases of the weak van der Waals interactions or the strong chemical crosslinks among flakes are also verified. Similar microstructural evolutions are found, which would be an intrinsic property of energy dissipation for graphene foams, independent of their structural factors.

5. Micro-mechanism of energy dissipation under single compression-tension load

Analyzing the microstructural evolution in both the large-strain compression-tension and the small-strain compression-tension
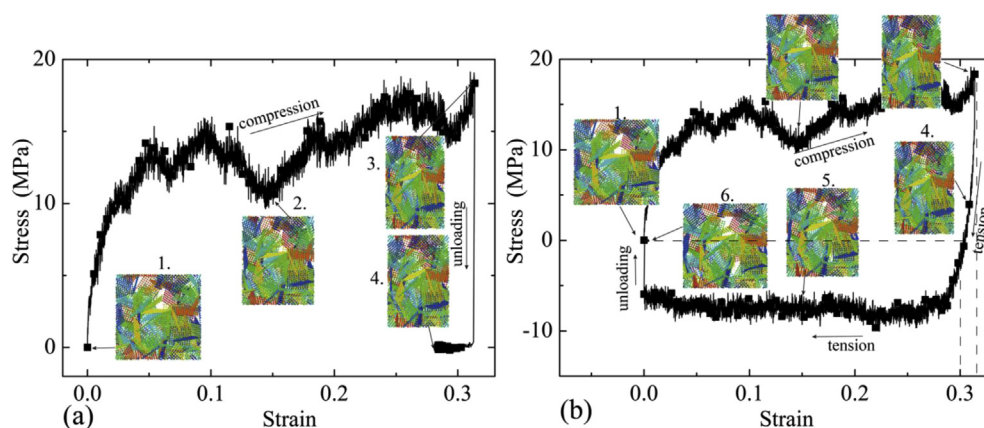
Fig. 4. The stress-strain constitutive relation of graphene foam materials. (a) Under a large-strain compression-unloading condition; (b) Under a large-strain compression-tension-unloading condition. The insets are some snapshots for understanding. (A colour version of this figure can be viewed online.)
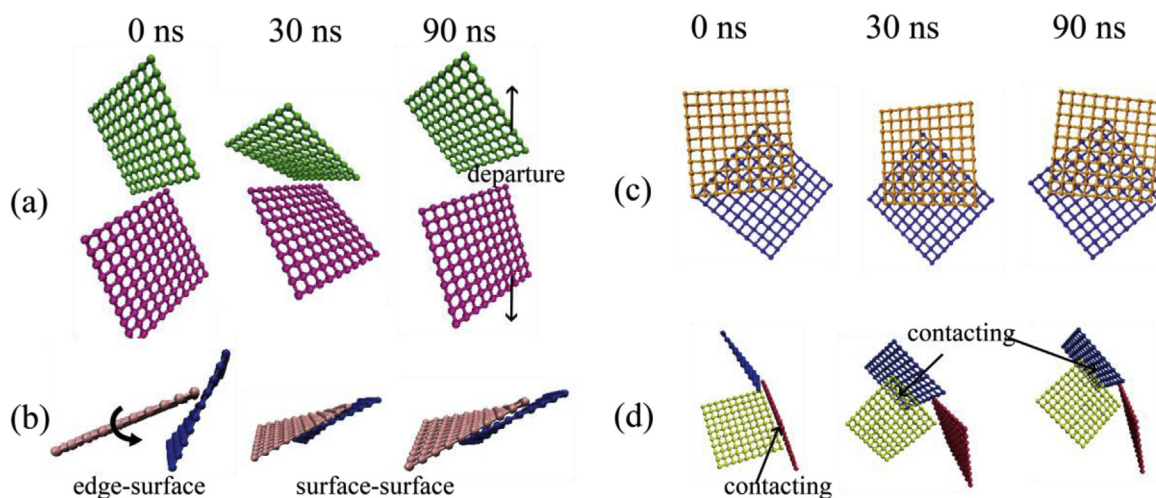

Fig. 5. Four kinds of microstructural evolutions in graphene foam materials system at the initial state of 0 ns, the compressive state of 30 ns and the final state after unloading at 90 ns. (A colour version of this figure can be viewed online.)

cases, we find three kinds of energy dissipative mechanisms essentially exist in the scale of graphene flakes, i.e., the flake rippling, relative sliding and impacting. Three sets of microstructural configurations of energy dissipation are extracted from the numerical calculations as shown in Fig. 6. The corresponding movies named "Rippling", "Sliding" and "Impacting" are given in Supplementary Materials, respectively.

Actually, rippling is an intrinsic property of graphene sheet itself, which would spontaneously happen due to thermal fluctuations [30]. Using molecular dynamic simulations, He et al. have also found ripples would form in a single layered graphene when it is stroked by a C60 molecule. The ripples formed by impacting would interact with the intrinsic ones activated by thermal fluctuations, leading to the noticeable diffraction and interference of ripples [31]. The dissipative mechanism of rippling, including the formation, propagation, diffraction and interference of ripples in flakes has been suggested initially by Debrupa et al. [20] to explain the dissipative behavior of a few-layered graphene membrane. In graphene foam materials formed by multi-layered graphene flakes, we first find the rippling behavior of flakes and the ripples of flakes could be constantly generated due to thermal actuation at a finite temperature, e.g., 300 K here, and impact from neighboring flakes induced by the external load. As shown in Fig. 6(a—c) and the movie

"Rippling", two flakes contact each other, wiggle to and fro constantly along with the externally cyclic load. During the process, flakes are warped owing to the ripples. Only slight ripple can be found in Fig. 6(a—c) due to the adopted stiff and small flakes in this simulation. If graphene foam materials consisting of relatively large and flexible flakes, ripples would be much obvious. An example is given in Fig. S1 in Supplementary Materials, in which each square flake has a side length 125 nm. For a monolayer graphene flake, ripples would propagate forward and vanish at the free edges or interfaces between two contacting sheets [31], during which energy would be dissipated. Considering the fact that GrFs are composed of a large number of flakes, we believe that rippling including the propagation, diffraction and interference of ripple waves in flakes should be one of the main channels to dissipate energy.

Sliding between two adjacent flakes, even partly or entirely folding itself to form surface/surface contact can also happen due to the inter-flake adhesion as shown in Fig. 6(d—f). In a real GrF, surface-surface contact is also the most ubiquitous microstructure observed in SEM and TEM experiments [1,32]. From Fig. 6(d—f) and the movie "Sliding" in Supplementary Materials, it is clearly shown that two flakes in a surface-surface contact configuration would slide against each other and move to and fro constantly under cyclic
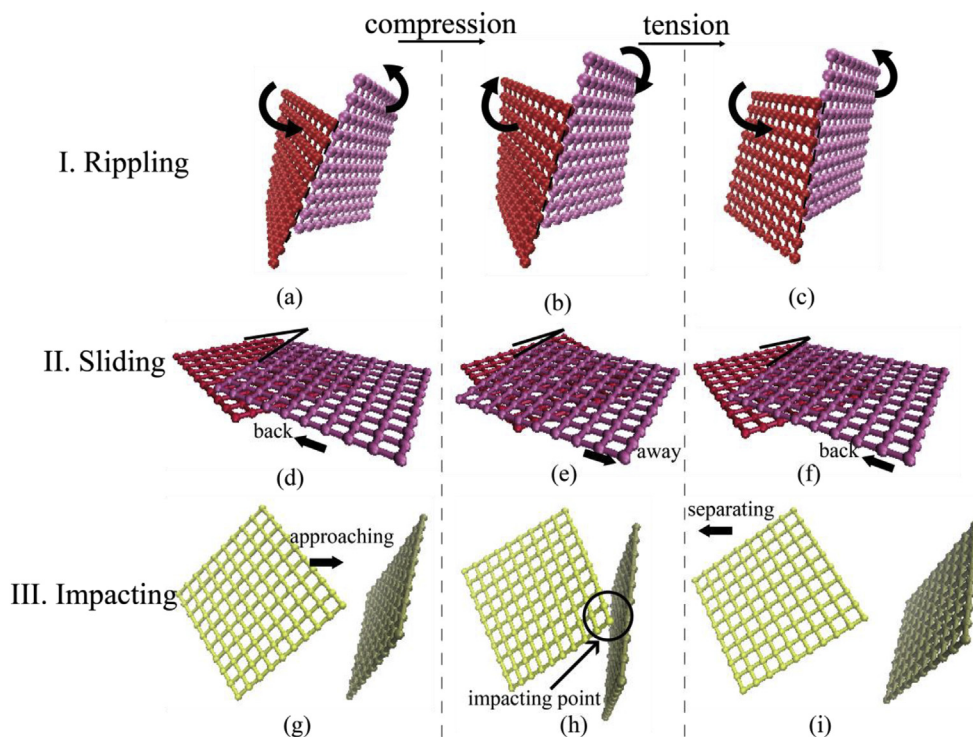
Fig. 6. Three kinds of dissipative mechanisms. (a–c) rippling, (d–f) sliding and (g–i) impacting. (A colour version of this figure can be viewed online.)

load. In this process, flakes are apt to rotate spontaneously to a more stable commensurate configuration with much higher friction and move with a stick-slip fashion like that in superlubricity [33] of graphene, which would induce considerable energy dissipation. Therefore, the relative sliding between laminated flakes in GrFs should be another strategy of energy dissipation. Similar dissipative mechanism has also been reported in the carbon nanotube-based network materials [29,34].

Impacting among flakes can not be avoided under cyclic load as shown in Fig. 6(g–i), and the movie "Impacting" in Supplementary Materials. Each collision event can be looked as an indentation or impacting test on a graphene sheet, as studied by He et al. [31]. The activated elastic waves would propagate outwards from the impacting point, which is an energy dissipative process as discussed above. In the collision process, the intrinsic wave activated by thermal fluctuations in a flake will be suppressed by the collision from neighbor flakes, which leads to energy dissipation too [20]. In addition, the microscopic collision among different flakes can also be viewed as an unstable attachment-detachment process, a similar process of which has been regarded as a main mechanism of energy dissipation in carbon nanotube networks [35]. Therefore, collision should be an important channel for energy dissipation in graphene foam materials since it happens as a microscopic event of high frequency.

It should be noted that, different from the first dissipative mechanism of ripple in a flake, the latter two mechanisms reflect a new channel of energy dissipation through the interaction among neighbor flakes, which has not been noticed before in the experimental or numerical graphene foam systems.

Besides the above three dissipative mechanisms, much larger-strain magnitude would induce rupture of the in-plane bonds or inter-flake chemical crosslinks as discussed in the study of fracture mode of GrFs [18,19], which can also induce energy dissipation.

The above three dissipative mechanisms are much different in systems under different loading conditions. For example, all three kinds of dissipative mechanisms can be identified easily in the case with large-strain loading, while in the small-strain loading case, only the slightly impacting between neighboring flakes can be found easily, sliding between laminated flakes and rippling of flakes are so weak that can not be identified in the simulations, see the movie "DMA.gif" or "small-strain-compression-unloading.gif" in Supplementary Materials; most of flake rearrangements can recover gradually due to the viscous damping behavior.

Since foam branches/walls are hollow structures, which are composed of multiple graphene flakes, the energy dissipation in the branch/wall scale, such as twisting, bending, or compression [15], is essentially the result of rippling, sliding or impacting of their constituent flakes.

6. Micro-mechanism of energy dissipation under compression-tension cyclic load

Systematic simulations under ten continuous compression-tension cycles are carried out. In each loading cycle, the sample is first uniaxially compressed to a maximum strain at the strain rate ~10^7 s^{-1} in the x-direction, during which zero pressure barostat remains in the other two directions. Then, the compressed sample is tensioned in the reverse direction to the initial size under the same condition. The dissipative energy in each cycle can be calculated numerically from the stress-strain curves. The stress-strain curves under cyclic load of ten times are plotted in Fig. 7(a–c) for three typical strain amplitudes 0.11, 0.31 and 0.52, respectively. It is found that no matter how much the magnitude is, the stress-strain curve of the first cycle is much different from those of the subsequent nine cycles. Furthermore, all the stress-strain curves of the subsequent nine cycles almost coincide with each other. Interestingly, such a feature has also been observed in real experiments [1,2,11], though chemical cross-links among flakes are not included in the present simulations.

In order to understand this point from the view of
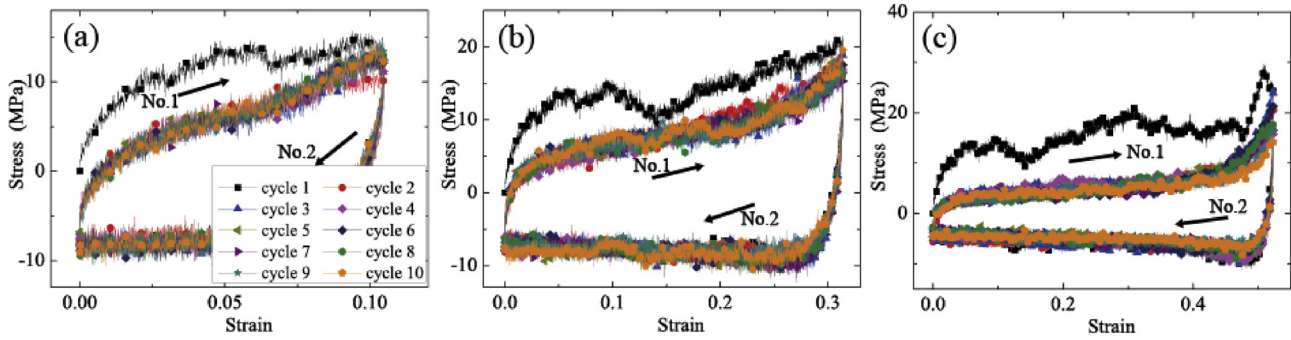
Fig. 7. The stress-strain curves of graphene foam materials under ten times large-strain compression-tension cycles. (a) The strain amplitude is 0.11. (b) The strain amplitude is 0.31. (c) The strain amplitude is 0.52. (A colour version of this figure can be viewed online.)

microstructural evolution, we exploit two parameters of the "mass center displacement" and "rotating angle" of flakes to measure the intensity of flake rearrangement in each loading cycle. Fig. 8 gives an overall comparison of flake rearrangement in the graphene foam materials between the starting state and the final one in each loading cycle. The flakes with displacement/rotating angle in a loading cycle larger than 2 nm/10° are marked red in the final state of the corresponding cycle. The two threshold values of 2 nm and 10° are chosen after many simulation trials, which can highlight the difference of flake rearrangement in single loading cycle and among successive loading cycles. The more flakes marked red in the system indicate more drastic flake rearrangement in the final state of the last loading cycle in contrast to the initial state of the first cycle. It is very obvious that the number of red flakes in the first loading cycle is much more than that in other ones, which indicates drastic flake rearrangement in the first loading cycle. More energy should be dissipated during the first cycle.

Details of microstructural evolution in each cycle are shown in Fig. 9, in which energy dissipation in each cycle can be demonstrated clearly. Fig. 9a shows the evolution of an initial edge-surface configuration, which evolves to be a surface-surface contact structure after large rotation of one flake in the first loading cycle.

Afterwards, the surface-surface contact structure keeps almost stable in the subsequent cycles. The large rotation and large displacement of flakes can also been observed during the first cycle in the other two configurations as shown in Fig. 9(b–c), which remain almost unchanged in the following nine cycles too. The microstructural evolution difference between the first cycle and the subsequent cycles should be the main cause that leads to the great difference of macroscopic stress-strain curve between the first loading cycle and the following ones.

The dissipative energy in each loading cycle can be measured from the area enveloped by the macroscopic stress-strain curve, which is shown in Fig. 10a. For a fixed strain amplitude, the dissipative energy defined as the energy dissipated per unit volume decreases from a larger value in the first loading cycle and tends to be a constant in the subsequent ones, the feature of which agrees well with that found in experiments [1,2,11]. The dissipative energy increasing with the strain amplitude in the same corresponding cycle number is also consistent with the observation in experiments [11], where a larger stress-strain hysteresis loop was obtained in the case with a larger strain amplitude but in the same cycle number.
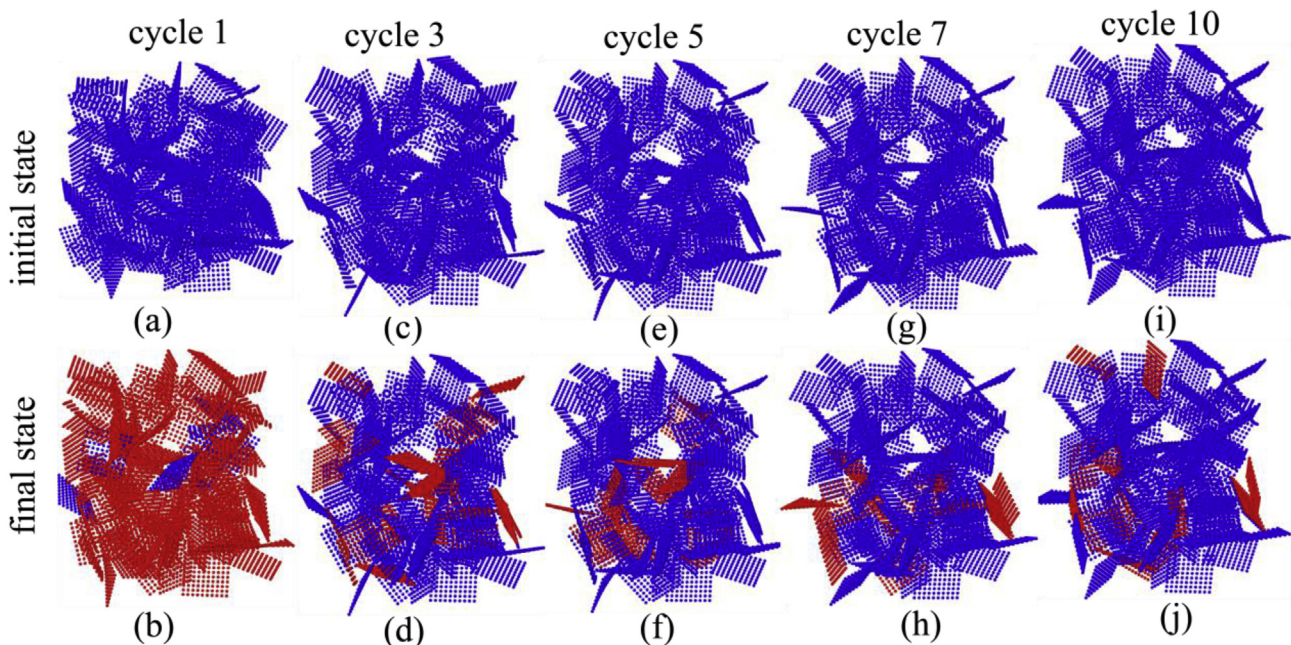
Fig. 8. Comparison between the starting state and the final state of graphene foam materials in each loading cycle. Here, the strain amplitude is 0.31. (a–b) cycle 1, (c–d) cycle 3, (e–f) cycle 5, (g–h) cycle 7 and (i–j) cycle 10. (A colour version of this figure can be viewed online.)
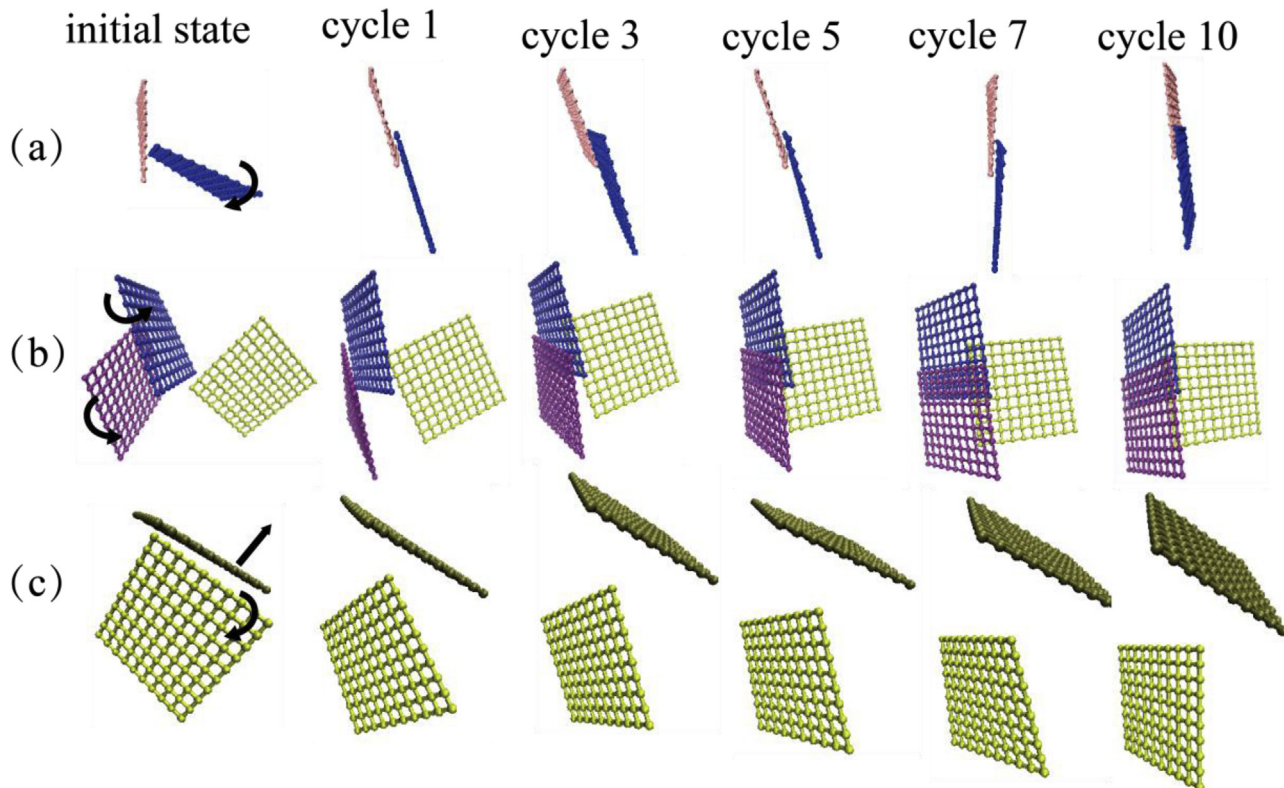
Fig. 9. Configuration of three typically microstructural evolutions at the final state of each loading cycle. (A colour version of this figure can be viewed online.)
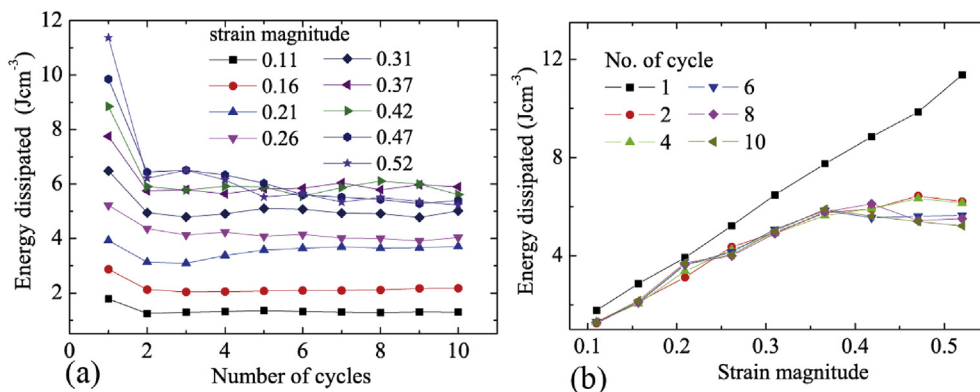

Fig. 10. Variation of the dissipative energy per unit volume. (a) As a function of the cycle number for a fixed strain amplitude. (b) As a function of the strain amplitude in the same number of cycles. (A colour version of this figure can be viewed online.)

## 7. Influencing factors of energy dissipation

Microstructures after ten loading cycles under strain amplitudes of 0.11, 0.31 and 0.52 are shown in Fig. 11(a–c), respectively. It is found that, as strain amplitude increases, a "stacking structure" composed of multiple flakes forms gradually in the foam system. During deformation, the stacking structure behaves like a rigid body with negligibly inside relative movement of flakes, see the Movie "cycle-loading-0.52.gif" in Supplementary Materials. As a result, many pores emerge and become larger and larger with the increase of strain amplitude, which are pointed by arrows in Fig. 11(a–c) and labeled as "small pores", "medium pores" and "big pores", respectively. The growth or shrinkage of pores should be another energy dissipative mechanism on the upper level of flakes.

The effect of loading rate on the energy dissipation of GrFs is also investigated. Five kinds of strain rates 10^6, 5×10^6, 10^7, 5×10^7 and 10^8 s^{-1} are adopted, respectively. The dissipative energy as a function of the loading rate is shown in Fig. 12. No matter how much the strain amplitude is, the dissipative energy increases monotonically with the increase of the loading rate. Such a result could be easily understood based on the dissipative mechanisms of rippling, sliding and impacting of flakes, which should be enhanced by a higher loading rate. The similar result of dissipative energy depending on the loading rate was reported for carbon nanotube network materials [36]. The effect of bending stiffness k_θ that ranges from 144.9 to 1292671 kcal·mol^{-1}·rad^{-2} to denote different layered graphene flakes, and the effect of the side length that ranges from 25 to 125 nm to denote different sizes of square flakes,
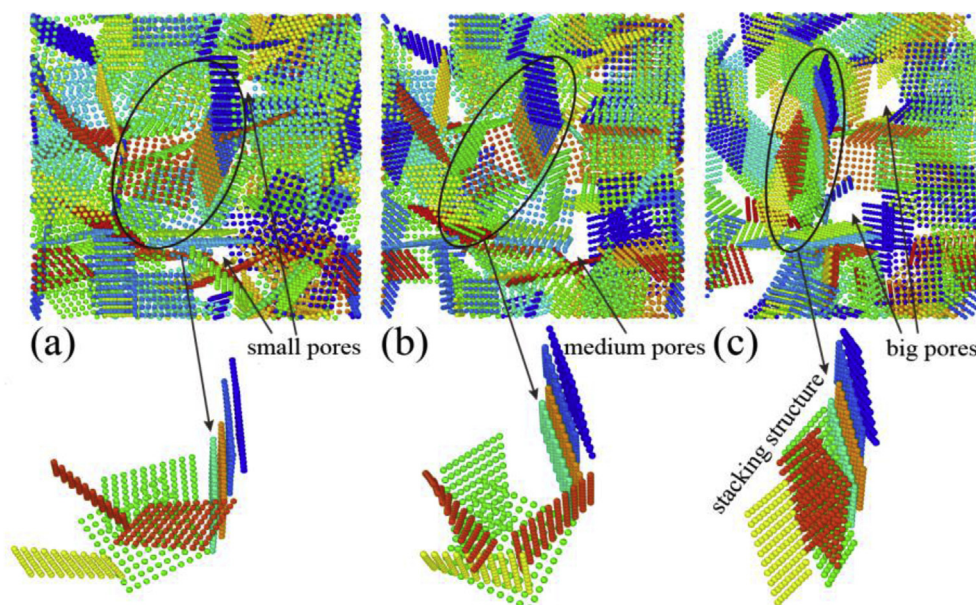
Fig. 11. The finally equilibrated microstructure of graphene foam materials after 10 loading cycles. (a) The strain amplitude is 0.11; (b) The strain amplitude is 0.31; (c) The strain amplitude is 0.52. A stacking structure is found during the loading cycle. (A colour version of this figure can be viewed online.)
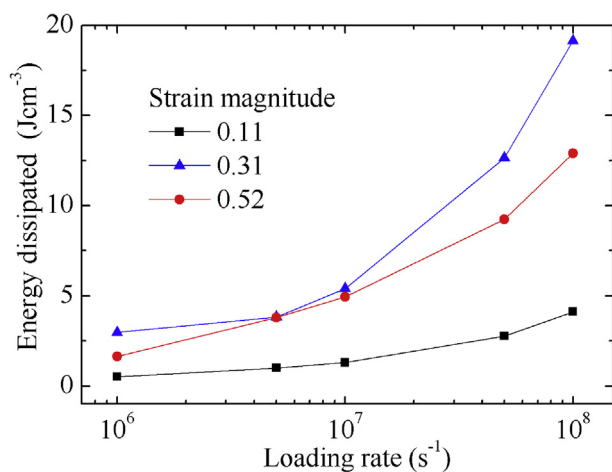
Fig. 12. The dissipative energy as a function of the loading rate. (A colour version of this figure can be viewed online.)

on the dissipative energy are further considered. Similar results are found. It means that the energy dissipative mechanism in GrFs is not influenced by the two parameters, i.e., the bending stiffness and the size of flakes. The three kinds of micro-mechanisms should coexist and the only difference is which one may account for larger proportion.

8. Conclusions

Based on the coarse-grained molecular dynamic simulation, the energy dissipative micro-mechanism of 3D graphene foam materials is investigated in this paper. The constitutive relation of the graphene foam materials is reproduced first under both small-strain loading-unloading and large-strain loading-unloading, which shows a typically visco-elastic plastic property and a strong energy dissipative capability. Four typically microstructural evolutions are mainly found, including the departure of two contacting flakes, transformation from edge-surface contacting configuration to the surface-surface one, the variation of contacting areas between two surface-surface contacting flakes and the change of contacting partners, which are irreversible for plastic deformation and can be partially restored for visco deformation. The energy dissipative micro-mechanisms are further disclosed under different loading forms, including single compression-tension load, and large-strain compression-tension cyclic load. Under single compression-tension load, the flake rippling, relative sliding and impacting would be three main energy dissipative mechanisms. In the case of large-strain compression-tension cyclic load, the dissipative energy in each cycle can be calculated numerically from the stress-strain curves. It is always found that the dissipative energy in the first cycle is much larger than that in the subsequent cycles, which is due to the drastic flake rearrangement in the first loading cycle and consistent with the experimental observations. In addition, as the strain amplitude increases, a "stacking structure" will form, which looks like a locally permanent plastic zone and would induce the growth or shrinkage of pores as another upper-level mechanism to dissipate energy too. The present study should not only deepen our understanding of the energy dissipative micro-mechanism of graphene foams but also be helpful for the design of novel multi-functional graphene-based materials and devices.

Competing financial interests

The authors declare no competing financial interests.

Appendix A. Supplementary data

Supplementary data related to this article can be found at https://doi.org/10.1016/j.carbon.2018.02.085.

References

[1] X. Xu, Q. Zhang, Y. Yu, W. Chen, H. Hu, H. Li, Naturally dried graphene aerogels with superelasticity and tunable Poisson's ratio, Adv. Mater. 28 (2016) 9223—9230.

[2] Y. Wu, N. Yi, L. Huang, T. Zhang, S. Fang, H. Chang, et al., Three-dimensionally bonded spongy graphene material with super compressive elasticity and near-zero Poisson's ratio, Nat. Commun. 6 (2015) 6141.

[3] L. Qiu, J.Z. Liu, S.L.Y. Chang, Y. Wu, D. Li, Biomimetic superelastic graphene-based cellular monoliths, Nat. Commun. 3 (2012) 1241.

[4] L. Qiu, B. Huang, Z. He, Y. Wang, Z. Tian, J.Z. Liu, et al., Extremely low density and super-compressible graphene cellular materials, Adv. Mater. 1701553 (2017) 1701553.

[5] F. Yavari, Z. Chen, A.V. Thomas, W. Ren, H.-M. Cheng, N. Koratkar, High sensitivity gas detection using a macroscopic three-dimensional graphene foam network, Sci. Rep. 1 (2011) 1—5.

[6] S. Chen, P. Bao, X. Huang, B. Sun, G. Wang, Hierarchical 3D mesoporous sili-con@graphene nanoarchitectures for lithium ion batteries with superior performance, Nano Res. 7 (2014) 85—94.

[7] H. Bi, X. Xie, K. Yin, Y. Zhou, S. Wan, L. He, et al., Spongy graphene as a highly efficient and recyclable sorbent for oils and organic solvents, Adv. Funct. Mater. 22 (2012) 4421—4425.

[8] Z. Chen, W. Ren, L. Gao, B. Liu, S. Pei, H.-M. Cheng, Three-dimensional flexible and conductive interconnected graphene networks grown by chemical vapour deposition, Nat. Mater. 10 (2011) 424—428.

[9] Q. Peng, Y. Li, X. He, X. Gui, Y. Shang, C. Wang, et al., Graphene nanoribbon aerogels unzipped from carbon nanotube sponges, Adv. Mater. 26 (2014) 3241—3247.

[10] Z. Qin, G.S. Jung, M.J. Kang, M.J. Buehler, The mechanics and design of a lightweight three-dimensional graphene assembly, Sci Adv 3 (1) (2017) e1601536.

[11] H. Hu, Z. Zhao, W. Wan, Y. Gogotsi, J. Qiu, Ultralight and highly compressible graphene aerogels, Adv. Mater. 25 (2013) 2219—2223.

[12] Y. Xu, K. Sheng, C. Li, G. Shi, Self-assembled graphene hydrogel via a one-step hydrothermal process, ACS Nano 4 (2010) 4324—4330.

[13] C. Zhu, TY-j Han, E.B. Duoss, A.M. Golobic, J.D. Kuntz, C.M. Spadaccini, et al., Highly compressible 3D periodic graphene aerogel microlattices, Nat. Commun. 6 (2015) 1—8.

[14] Q. Zhang, F. Zhang, S.P. Medarametla, H. Li, C. Zhou, D. Lin, 3D Printing of Graphene Aerogels, 2016, pp. 1702—1708.

[15] P. Nautiyal, B. Boesl, A. Agarwal, Harnessing three dimensional anatomy of graphene foam to induce superior damping in hierarchical polyimide nano-structures, Small (2016) 1603473.

[16] Ja Baimova, L.K. Rysaeva, B. Liu, S.V. Dmitriev, K. Zhou, From flat graphene to bulk carbon nanostructures, Phys. Status Solidi 252 (2015) 1502—1507.

[17] C. Wang, C. Zhang, S. Chen, The microscopic deformation mechanism of 3D graphene foam materials under uniaxial compression, Carbon 109 (2016) 666—672.

[18] A. Nieto, B. Boesl, A. Agarwal, Multi-scale intrinsic deformation mechanisms of 3D graphene foam, Carbon 85 (2015) 299—308.

[19] D. Pan, C. Wang, T.C. Wang, Y. Yao, Graphene foam: uniaxial tension behavior and fracture mode based on a mesoscopic model, ACS Nano 11 (9) (2017) 8988—8997.

[20] D. Lahiri, S. Das, W. Choi, A. Agarwal, Unfolding the damping behavior of multilayer graphene membrane in the low-frequency regime, ACS Nano 6 (2012) 3992—4000.

[21] S. Cranford, M.J. Buehler, Twisted and coiled ultralong multilayer graphene ribbons, Model. Simulat. Mater. Sci. Eng. 19 (2011) 054003.

[22] L. Ruiz, W. Xia, Z. Meng, S. Keten, A coarse-grained model for the mechanical behavior of multi-layer graphene, Carbon 82 (2015) 103—115.

[23] S. Zhu, Y. Huang, T. Li, Extremely compliant and highly stretchable patterned graphene, Appl. Phys. Lett. 104 (2014).

[24] J.-J. Shang, Q.-S. Yang, X. Liu, New coarse-grained model and its imple-mentation in simulations of graphene assemblies, J. Chem. Theor. Comput. 13 (2017) 3706—3714.

[25] M. Dienwiebel, G.S. Verhoeven, N. Pradeep, J.W.M. Frenken, J.A. Heimberg, H.W. Zandbergen, Superlubricity of graphite, Phys. Rev. Lett. 92 (2004), 126101—1.

[26] S.J. Chae, F. Güneş, K.K. Kim, E.S. Kim, G.H. Han, S.M. Kim, et al., Synthesis of large-area graphene layers on poly-nickel substrate by chemical vapor deposition: wrinkle formation, Adv. Mater. 21 (2009) 2328—2333.

[27] Y. Tao, X. Xie, W. Lv, D.-M. Tang, D. Kong, Z. Huang, et al., Towards ultrahigh volumetric capacitance: graphene derived highly dense but porous carbons for supercapacitors, Sci. Rep. 3 (2013) 2975.

[28] S. Plimpton, Fast Parallel algorithms for short-range molecular dynamics, J. Comput. Phys. 117 (1) (1995) 1—19.

[29] Q.L. Liu, M. Li, Y.Z. Gu, S.K. Wang, Y.Y. Zhang, Q.W. Li, et al., Interlocked CNT networks with high damping and storage modulus, Carbon 86 (2015) 46—53.

[30] A. Fasolino, J.H. Los, M.I. Katsnelson, Intrinsic ripples in graphene, Nat. Mater. 6 (2007) 858—861.

[31] Y.Z. He, H. Li, P.C. Si, Y.F. Li, H.Q. Yu, X.Q. Zhang, et al., Dynamic ripples in single layer graphene, Appl. Phys. Lett. 98 (2011) 2012—2015.

[32] R. Zhang, Y. Cao, P. Li, X. Zang, P. Sun, K. Wang, et al., Three-dimensional porous graphene sponges assembled with the combination of surfactant and freeze-drying, Nano Res. 7 (2014) 1477—1487.

[33] A.E. Filippov, M. Dienwiebel, J.W.M. Frenken, J. Klafter, M. Urbakh, Torque and twist against superlubricity, Phys. Rev. Lett. 100 (2008) 1—4.

[34] C. Wang, L. Wang, Z. Xu, Enhanced mechanical properties of carbon nanotube networks by mobile and discrete binders, Carbon 2013 (64) (2013) 237—244.

[35] X. Yang, P. He, H. Gao, Modeling frequency- and temperature-invariant dissipative behaviors of randomly entangled carbon nanotube networks un-der cyclic loading, Nano Res. 4 (12) (2011) 1191—1198.

[36] S. Pathak, E.J. Lim, P.P. Abadi, S. Graham, B.A. Cola, J.R. Greer, Higher recovery and better energy dissipation at faster strain rates in carbon nanotube bun-dles: an in-situ study, ACS Nano 6 (3) (2012) 2189—2197.